Proceedings 10th NUMGE 2023
10th European Conference on Numerical Methods in Geotechnical Engineering
Zdravkovic L, Kontoe S, Taborda DMG, Tsiampousi A (eds)

https://doi.org/10.53243/NUMGE2023-155

Numerical performance of different order explicit integration schemes with substepping and automatic error control

M. Lloret-Cabot[1], D. Sheng[2]

[1]*Department of Engineering, University of Durham, Durham, UK*
[2] *Department of Civil Engineering, University of Technology Sydney, Sydney, Australia*

ABSTRACT: The numerical integration of the incremental stress-strain relations of a constitutive model for soils plays a central role in the overall computational performance of geotechnical finite element analyses and it is, therefore, desirable to have an efficient integration scheme that ensures accurate solutions with a reasonable computational effort. Substepping integration schemes with automatic error control are precisely aimed at providing such numerical efficiency. Against this background, this paper discusses the numerical performance of low and high order accurate explicit substepping and implicit integration schemes when integrating, numerically, the constitutive relations of the Modified Cam Clay (MCC) for typical stress paths. The discussion is presented in the context of the performance maps which are useful and simple verification tools to check that the algorithm performs as expected at a single integration as well as when the substepping is active and, in addition, provide information about the appropriate value of the tolerance to be used in the substepping scheme (*STOL*) to reach a prescribed level of accuracy, while also anticipating the associated approximate computational cost.

Keywords: Integration schemes, Explicit, Substepping, automatic error control

1 INTRODUCTION

This paper studies and compares the computational performance of implicit and explicit algorithms for the numerical integration of the stress-strain relations of critical state constitutive models for saturated soils. As implicit scheme, the paper considers the conventional single-step first other accurate backward Euler integration scheme (BE1) which has been used extensively in the literature (e.g. Belytschko et al., 2000; Coombs et al., 2010, 2011; Jeremic & Sture, 1997; Pérez-Foguet et al., 2001; Simo & Taylor, 1986). Due to their popularity in the context of geotechnical engineering (Farias et al., 2009; Lloret-Cabot et al., 2016; Pérez-Foguet et al., 2001; Sloan, 1987; Sloan et al., 2001), various different order accurate explicit substepping schemes with automatic error control are also considered. The computational comparison presented focuses on two key aspects in the numerical integration of a constitutive model: accuracy and efficiency. Comparisons between implicit and explicit methods for geotechnical problems have been a common topic of discussion (e.g. Pedroso & Farias, 2005; Potts & Ganendra, 1994) and it is generally accepted that explicit substepping algorithms allow for a higher accuracy than implicit schemes, at the expense of a larger computational cost. In this context, Oliver et al., (2008) show that implicit integration schemes are often unconditionally stable and this characteristic tends to allow for larger lengths of the step to be integrated (hence, the number of required steps can be smaller). Furthermore, the initial value problem (IVP) to be solved in each step is typically highly non-linear when the unknown are expressed in an implicit formulation which requires advanced iterative procedures typically demanding smaller step lengths (which may result in ill-conditioned systems with no convergence i.e. less robust). In contrast, explicit schemes are often conditionally stable which translates into smaller lengths of the step to be integrated and hence a larger number of steps which, in turn, tends to increase the associated computational cost (Oliver et al., 2008). The IVP to be solved explicitly is typically found to be quasi linear in terms of the unknowns which facilitates the solution significantly (i.e. increased robustness).

This paper builds on this previous knowledge on implicit and explicit integration schemes with the aim to provide some further rationale on their respective suitability for finite element analysis. To reach this goal the paper analyses the computational performance of five integration schemes, including the fully implicit first order accurate backward Euler and a family of different order accurate explicit substepping schemes with automatic error control.

2 FORMULATION OF THE PROBLEM

The numerical integration of a critical state model involves the solution of an ordinary differential system of equations (ODE). For the Modified Cam Clay (MCC), this ODE can be written as (Sloan et al., 2001):

$$\begin{cases} \mathrm{d}\boldsymbol{\sigma}' = \mathbf{D}\mathrm{d}\boldsymbol{\varepsilon} \\ \mathrm{d}p'_0 = \mathrm{d}\lambda B \\ \mathrm{d}v = -v\mathrm{d}\varepsilon_v \end{cases} \quad (1)$$

where d**σ'** is the effective stress vector (difference between the total stress d**σ** and pore water pressure **I**du, where **I** is the identity matrix), d**ε** is the strain vector, **D** is the elastic/elasto-plastic matrix (which takes the elastic form $\mathbf{D_e}$ when no plastic yielding occurs) or the elasto-plastic $\mathbf{D_{ep}}$ (for plastic yielding), dp_0' is the mechanical hardening parameter, dλ is the plastic multiplier, B is a scalar, v is the specific volume and dε_v is the volumetric strain (see also Lloret-Cabot et al., 2016).

Equation 1 defines an IVP to be solved via an integration scheme when knowing the variation of strain, the initial effective stresses and the initial hardening parameter. Different implicit and explicit formulations to solve this IVP are presented next.

3 EXPLICIT SUBSTEPPING SCHEMES

Since the work of Sloan (1987), the application of substepping integration schemes to geotechnical finite element analysis has led to a large number of studies involving saturated (e.g. Farias et al., 2009; Lloret-Cabot et al., 2016; Pedroso & Farias, 2005; Pérez-Foguet et al., 2001; Sheng et al., 2002; Sloan et al., 2001) and unsaturated soil conditions (e.g. Lloret-Cabot et al., 2021; Pedroso et al., 2008; Sheng et al., 2003; Sołowski & Gallipoli, 2010). However, the majority of these works have focussed on the use of the explicit modified Euler with substepping, with little research on higher order integration schemes (e.g. Sołowski et al., 2012; Lloret-Cabot & Sheng, 2022). With the aim to offset this situation, four different order accurate explicit substepping strategies with automatic error control are presented in this section to integrate the IVP defined by Equation 1. Details covering specific aspects of the explicit algorithmic formulation such as elastic-plastic transitions, yield curve intersection and correction of stresses back to the yield surface are given elsewhere (e.g. Potts & Gens, 1985; Sloan et al., 2001). Equation 1 can be re-written as:

$$\begin{cases} \frac{\mathrm{d}\boldsymbol{\sigma}\prime}{\mathrm{d}T} \cong \mathbf{D_{ep}}\Delta\boldsymbol{\varepsilon} = \mathbf{D_e}\Delta\boldsymbol{\varepsilon} - \Delta\lambda\mathbf{D_e}\mathbf{b} \\ \frac{\mathrm{d}p\prime_0}{\mathrm{d}T} \cong \Delta\lambda B \\ \frac{\mathrm{d}v}{\mathrm{d}T} = -v\Delta\varepsilon_v \end{cases} \quad (2)$$

where T is a pseudo-time to control the integration of the strain increment $\Delta\boldsymbol{\varepsilon}$ (with $T = 0$ at the start and $T = 1$ at the end) and,

$$\Delta\lambda = \frac{\boldsymbol{a}^T\mathbf{D_e}\Delta\boldsymbol{\varepsilon}}{A - \boldsymbol{a}^T\mathbf{D_e}\Delta\boldsymbol{b}} \quad (3)$$

where the subscript "T" indicates transposed, $\boldsymbol{a}$ is the derivative of the yield curve with respect to effective stress, $\boldsymbol{b}$ the derivative of plastic potential with respect to effective stress and A is a scalar.

Integrating Equation 2 over T by knowing the initial state of the soil at $T = 0$ (i.e. n-1) and the imposed strain increment $\Delta\boldsymbol{\varepsilon}$, values of the effective stress, mechanical hardening parameter and specific volume can be found at n (i.e. $T = 1$):

$$\begin{cases} \boldsymbol{\sigma}'_n = \boldsymbol{\sigma}'_{n-1} + \sum_{i=1}^{s} b_i\,\Delta\boldsymbol{\sigma}'_i \\ p'_{0n} = p'_{0n-1} + \sum_{i=1}^{s} b_i\,\Delta p'_{0i} \\ v_n = v_{n-1}\,exp(-\Delta T_n\Delta\varepsilon_v) \end{cases} \quad (4)$$

where s is the number of integration stages, the values of the coefficients b_i are given in Tables 1, 2, 3 and 4 (for RK12, RK23, RK34 and RK45 respectively) and

$$\left.\begin{array}{l} \Delta\boldsymbol{\sigma}'_i = \mathbf{D_{ep}}(\hat{\boldsymbol{\sigma}}'_i, \hat{p}'_{0i}, \hat{v}_i)\Delta\boldsymbol{\varepsilon}_n \\ \Delta p'_{0i} = \Delta\lambda(\hat{\boldsymbol{\sigma}}'_i, \hat{p}'_{0i}, \hat{v}_i, \Delta\boldsymbol{\varepsilon}_n)B(\hat{\boldsymbol{\sigma}}'_i, \hat{p}'_{0i}, \hat{v}_i) \\ \Delta\boldsymbol{\varepsilon}_n = \Delta T_n\Delta\boldsymbol{\varepsilon} \end{array}\right\} \quad (5)$$

for $i = 1, \ldots, s$ and with,

$$\left.\begin{array}{l} \hat{\boldsymbol{\sigma}}'_i = \boldsymbol{\sigma}'_{n-1} + \sum_{k=1}^{i-1} a_{ik}\,\Delta\boldsymbol{\sigma}'_k \\ \hat{p}'_{0i} = p'_{0n-1} + \sum_{k=1}^{i-1} a_{ik}\,\Delta p'_{0k} \\ \hat{v}_i = v_{n-1}\,exp\left(-\sum_{k=1}^{i-1} a_{ik}\,\Delta T_n\Delta\varepsilon_v\right) \end{array}\right\} \quad (6)$$

for $i = 1, \ldots, s$ and for a_{ik} as given in the tables below.

Single-step explicit integration schemes do not control the size of the integration scheme and, hence, the advancement of the solution is carried out at once for each increment size. This contrasts with explicit substepping integrations schemes where the advancement of the solution is controlled by estimating the local truncation error REL as the difference in the numerical solutions from the higher and lower order schemes:

$$REL = max\left\{\frac{[(\hat{\boldsymbol{\sigma}}\prime - \boldsymbol{\sigma}\prime)^T(\hat{\boldsymbol{\sigma}}\prime - \boldsymbol{\sigma}\prime)]^{1/2}}{[(\hat{\boldsymbol{\sigma}}\prime)^T(\hat{\boldsymbol{\sigma}}\prime)]^{1/2}}, \frac{|\hat{p}_0\prime - p_0\prime|}{\hat{p}_0\prime}\right\} \quad (7)$$

where the variables with a hat correspond to the higher order accurate approximations. If REL is larger/smaller than the substepping tolerance $STOL$, the current step/substep size is reduced/increased according to:

$$(\Delta T)_{i+1} = r(\Delta T)_i \quad (8)$$

where $r \in [0.1, 1.1]$ (to control the change in size during two consecutive substeps, see Sloan et al., 2001). Its expression for the RK12, RK23, RK34 and RK45 is, respectively:

$$r \cong 0.9 \left(\frac{STOL}{REL}\right)^{1/2} \quad (9)$$

$$r \cong 0.9 \left(\frac{STOL}{REL}\right)^{1/3} \quad (10)$$

$$r \cong 0.9 \left(\frac{STOL}{REL}\right)^{1/4} \quad (11)$$

$$r \cong 0.9 \left(\frac{STOL}{REL}\right)^{1/5} \quad (12)$$

Tables 1, 2, 3, 4 and 5 gives the values of b_i and a_{ik} for Equations 4 and 6, respectively, for the RK12, RK23, RK34 and RK45.

Table 1. Coefficients for the RK12 scheme (Sloan et al., 2001)

s	a_{ik}	$\widehat{\boldsymbol{b}_i}$	b_i
1		1/2	1
2	1	1/2	0

Table 2. Coefficients for the RK23 scheme (Fehlberg, 1969)

s	a_{ik}		$\widehat{\boldsymbol{b}_i}$	b_i
1			1/6	1/2
2	1		1/6	1/2
3	1/4	1/4	2/3	0

Table 3. Coefficients for the RK34 scheme (Fehlberg, 1969)

s	a_{ik}				$\widehat{\boldsymbol{b}_i}$	b_i
1					43/288	1/6
2	1/4				0	0
3	4/81	32/81			243/416	27/52
4	57/98	-432/343	1053/686		343/1872	49/156
5	1/6	0	27/52	49/156	1/12	0

Table 4. Coefficients for the RK45 scheme (Dormand and Prince, 1980)

s	a_{ik}					$\widehat{\boldsymbol{b}_i}$	b_i
1						19/216	31/540
2	1/5					0	0
3	3/40	9/40				100/2079	190/297
4	3/10	-9/10	6/5			-125/216	-145/108
5	226/729	-25/27	880/729	55/729		81/88	351/220
6	-181/270	5/2	-266/297	-91/27	189/55	5/56	1/20

Inspection of these tables shows that the number of stages s for the RK12, RK23, RK34 and RK45 is 2, 3, 5 and 6, respectively. This aspect is important here because it influences the overall computational cost of the substepping scheme, as discussed later.

4 IMPLICIT INTEGRATION SCHEMES

This section summarises the first order fully implicit backward Euler (BE1) integration scheme used to solve Equation 1. Further details on implicit algorithms, including derivatives can be found elsewhere, (e.g. Simo & Taylor (1986), Jeremic & Sture (1997)). Similar to the explicit susbtepping integration schemes discussed earlier, Equation 2 can be integrated implicitly over T when knowing the initial state of the soil at n-1 (i.e. quantities $\boldsymbol{\sigma}'_{n-1}$ and p'_{0n-1}) and the imposed increment of strain $\Delta\boldsymbol{\varepsilon}$. The problem to be solved can be written as:

$$\begin{cases} \boldsymbol{\sigma}'_n + \Delta\lambda \mathbf{D}_\mathbf{e}\boldsymbol{b} = \boldsymbol{\sigma}'_{n-1} + \mathbf{D}_\mathbf{e}\Delta\boldsymbol{\varepsilon} \\ p'_{0n} - \Delta\lambda B = p'_{0n-1} \\ f(\boldsymbol{\sigma}'_n, p'_{0n}) = 0 \end{cases} \quad (13)$$

where f is the yield curve of the MCC evaluated at n.

The unknowns $\mathbf{x}$ in in the previous equation are the effective stress, the mechanical hardening parameter and the plastic multiplier at n. The residuals are:

$$\boldsymbol{r} = \begin{pmatrix} \boldsymbol{\sigma}'_n + \Delta\lambda \mathbf{D}_\mathbf{e}\boldsymbol{b} - \mathbf{D}_\mathbf{e}\Delta\boldsymbol{\varepsilon} - \boldsymbol{\sigma}'_{n-1} \\ p'_{0n} - \Delta\lambda B - p'_{0n-1} \\ f(\boldsymbol{\sigma}'_n, p'_{0n}) \end{pmatrix} \quad (14)$$

In order to solve this nonlinear problem, the residuals are minimised with an iterative method (e.g. Newton-Raphson, NR) for which the jacobian matrix of the residuals $\mathbf{J}$ is needed:

$$\mathbf{J} = \begin{pmatrix} \mathbf{I}_{\boldsymbol{\sigma}\prime} - \Delta\lambda \mathbf{D}_\mathbf{e} \frac{\partial \boldsymbol{b}}{\partial \boldsymbol{\sigma}\prime} & \Delta\lambda \mathbf{D}_\mathbf{e} \frac{\partial \boldsymbol{b}}{\partial p\prime_0} & \mathbf{D}_\mathbf{e}\boldsymbol{b} \\ -\Delta\lambda \frac{\partial B}{\partial \boldsymbol{\sigma}\prime} & 1 - \Delta\lambda \frac{\partial B}{\partial p\prime_0} & -B \\ \boldsymbol{a}^T & \frac{\partial f}{\partial p\prime_0} & 0 \end{pmatrix} \quad (15)$$

where $\mathbf{a}$, A and B were introduced earlier and $\mathbf{I}$ is the identity matrix.

5 VERIFICATION AND COMPUTATIONAL ASPECTS

Although it is possible to formulate a substepping scheme in terms of *absolute* error (Lloret-Cabot et al., 2017), the work in this paper is on the *relative* error. In this context, it is useful to distinguish between the *local* relative error e (error incurred by the numerical scheme in the integration of a single substep) and the *cumulative* relative error E (the accumulation of local relative error over a number of substeps). The first aspect to check is

if the relative error incurred in the integrated variables of the model behaves correctly in a single substep (i.e. local relative error *e*). Once this has been checked, the error behaviour can be studied over many substeps (i.e. cumulative relative error *E*). Studying the behaviour of *e* with an explicit substepping scheme is equivalent to consider that *STOL* = 1. Different values of *STOL* should be considered when analysing the behaviour of *E*.

A numerical test is considered in this paper to study the behaviour of the error. This test assumes axisymmetric conditions and considers an initial stress state on the yield curve (at zero deviatoric stress) so that any increase in effective stress produces plastic yielding. The variation of the error is investigated for given finite equal variations of axial strain and radial strain $\Delta\varepsilon_a = \Delta\varepsilon_r \approx \Delta\varepsilon_v/3$, with $\Delta\varepsilon_v = 10^{-06}$ to 0.1. The MCC constants and initial state considered are indicated in Table 5. The tolerance associated with the yield surface *FTOL* is 10^{-12} (and is the same value of tolerance used in the iterative NR method in BE1).

Table 5. Values of soil constants and initial state for the MCC simulations for Test A

$\lambda = 0.12$	$\upsilon = 0.33^{(*)}$	$q = 0$ kPa
$\kappa = 0.05$	$M = 1.20$	$p' = 50$ kPa
$N = 2.00$		$p_0' = 50$ kPa

(*) Poisson's ratio

5.1 The relative local error, e

The behaviour of the error should be analysed in the integrated variables which, in this case, are $\boldsymbol{\sigma}'$ and p_0'. The local relative error in these variables (for a given $\Delta\boldsymbol{\varepsilon}$) can be computed by comparing the numerical solution obtained from a particular integration scheme against an accurate (or analytical) solution which will be referred here to as *reference* ("ref" in Equations 16-17).

$$e_{\boldsymbol{\sigma}'} = \frac{\left\{(\boldsymbol{\sigma}'_{ref}-\boldsymbol{\sigma}')^T(\boldsymbol{\sigma}'_{ref}-\boldsymbol{\sigma}')\right\}^{1/2}}{\left\{(\boldsymbol{\sigma}'_{ref})^T(\boldsymbol{\sigma}'_{ref})\right\}^{1/2}} \quad (16)$$

$$e_{p'_0} = \frac{|p'_{0ref}-p'_0|}{p'_{0ref}} \quad (17)$$

Local accuracy in each numerical method is assessed by plotting the local error in $\boldsymbol{\sigma}'$ and p_0' against the size of $\Delta\boldsymbol{\varepsilon}$. All plots use logarithmic scales in both axes to verify that the gradient of the best-fitted straight line through a particular set of error results corresponds to order of accuracy of the integration scheme used.

Figure 1 illustrates the local relative error in terms of $\boldsymbol{\sigma}'$ (Figure 1a) and p_0' (Figure 1b). The computed relative error is indicated by symbols and each dashed line shows the best-fitted straight line through the corresponding *e* from results of a particular integration scheme (these lines are referred to hereafter as *local error lines* as defined in Lloret and Sheng, 2022). The expression of a local error line in terms of the substep size *h* can be written as (assuming no cancellation):

$$e \approx ch^{p+1} \quad (18)$$

where *p* is the known order of the integration scheme and *c* is a constant. Equation 18 indicates that the local error line of a substepping scheme of order *p* will have a gradient of *p* + 1 when plotting the local relative error *e* against the step size *h* as demonstrated in Figure 1 for all six single-step integrations schemes considered. Inspection of Figure 1 confirms that, as expected, a first order local accuracy is achieved by RK1 and BE1. Interestingly, for an extremely exaggerated increment size ($\Delta\varepsilon_v \approx 0.6$), all integration schemes reach a similar value of *e* which confirms that this strain increment size is too large to show differences in accuracy between the various methods considered (and suggesting that smaller increment sizes should be used, see Figures 1a and 1b).

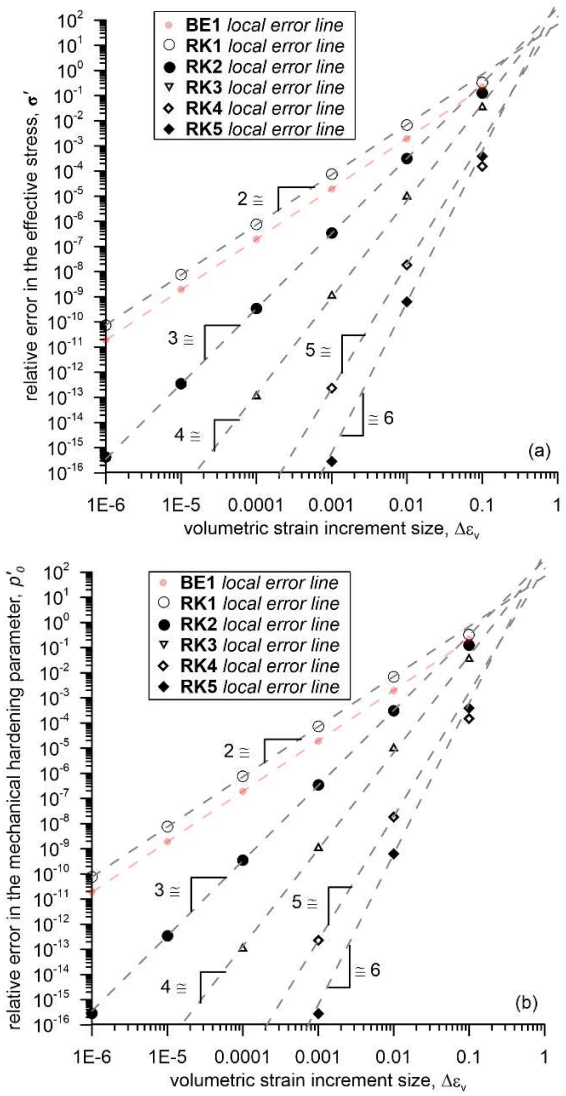

Figure 1. Local relative error against volumetric strain increment size for a single $\Delta\varepsilon_v$: (a) effective stress $\boldsymbol{\sigma}'$; (b) mechanical hardening parameter p_0'.

5.2 *The cumulative error, E*

After checking that integration at a single-step performs correctly, the verification of the numerical performance of the explicit substepping schemes over several substeps must be checked. As suggested in Lloret-Cabot et al. (2016), this can be studied by looking at the behaviour of the cumulative relative error *E* when the substepping is active.

Assuming *n* equal-sized substeps of size *h*, the cumulative relative error can be expressed as:

$$E \approx nch^{p+1} = Hch^{p} \qquad (19)$$

where *H* is the size of the total increment integrated i.e. *H*=*hn*. Equation 19 indicates that the final cumulative relative error approximately lies on a straight line when plotted against the substep size *h* in a log-log scale, having gradient 2, 3, 4 or 5 for the RK12, RK23, RK34 and RK45, respectively. Hence, Equation 19 defines another error line of gradient *p* referred to hereafter as *cumulative error line* (see also Lloret and Sheng, 2022).

Based on Equation 19 and considering the way the substepping scheme is formulated, Lloret-Cabot et al., (2016) propose a powerful form of plotting the computational outcomes from a substepping integration scheme (referred to as the *performance maps*). This graphical representation of the numerical outputs from substepping integration schemes is useful for studying their overall computational performance. The first performance map presented here represents *E* against the number of substeps *n* for different strain increment sizes (Figure 2a). The second represents *E* against the value of *STOL* for different strain increment sizes (Figure 2b). Note that both plots are only for the RK12 with substepping but similar results are obtained for the higher order substepping schemes considered (see Lloret-Cabot and Sheng, 2022).

Figure 2a shows how *n* influences the cumulative relative error in the effective stress when integrating volumetric strain increment $\Delta\varepsilon_v$. Inspection of Figure 2a shows that when *n* increases (due to a more restrictive *STOL*) the value of *E* tends to reduce. The rate of such reduction is defined by Equation 9, 10, 11 or 12 (so it can be verified) by plotting the error results of the corresponding integration scheme in the ln*E*:ln*n* plane. Figure 2a demonstrate this for the RK12.

Figure 2b illustrates the effect of varying *STOL* in *E* when integrating a given volumetric strain increment $\Delta\varepsilon_v$. As expected, reducing *STOL* leads to a reduction in the substep size $\delta\varepsilon_v$ which, in turn, leads to a smaller value of *e* in each individual substep of this size. A reduction in *E* is hence also expected for smaller *STOLs* once the full increment has been integrated. However, this reduction in *E* with decreasing *STOL* is only apparent when the substepping strategy has been activated (see Figure 2b). The constant (horizontal) variation of *E* with *STOL* indicates that the current substep size fulfils the restriction imposed by *STOL* and hence no substepping is needed. In contrast to these horizontal segments, a 1:1 gradient variation of *E* with *STOL* is observed in other parts of the plot indicating that substepping is active. This change from no substepping to substepping is identified by a sharp change in the error behaviour (which has been indicated in the plot by point Y). Note that the error values for the BE1 result in a vertical segment at *STOL* = 1.

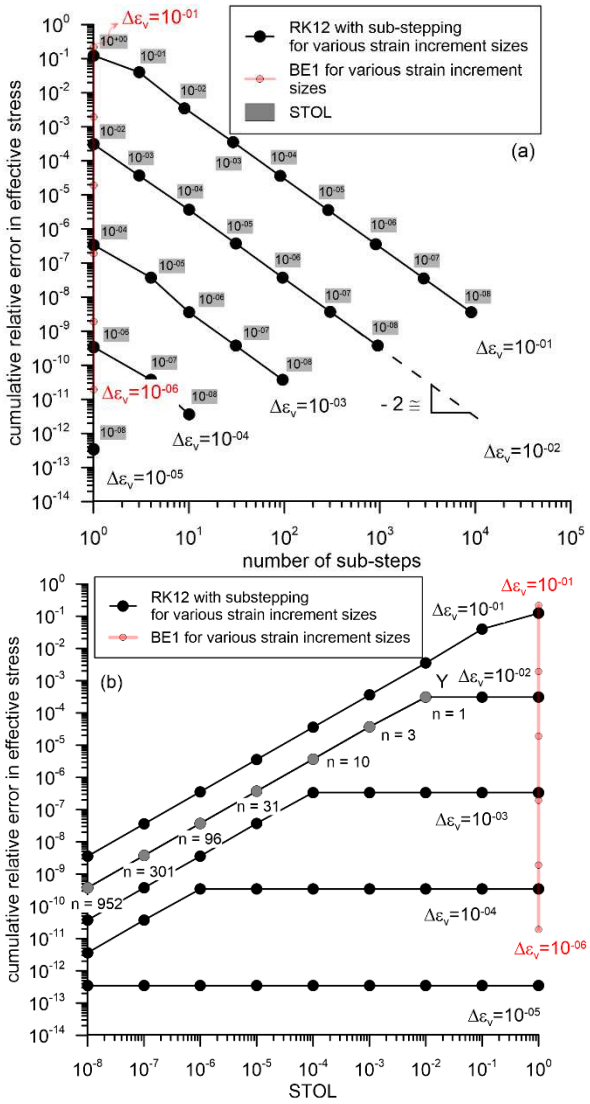

Figure 2. Performance maps for the RK12; (a) Cumulative relative error behaviour against number of substeps for an elasto-plastic volumetric strain increment (b) Cumulative relative error behaviour against STOL for an elasto-plastic volumetric strain increment.

6 CONCLUSIONS

Six integration schemes of different accuracy including explicit and implicit formulations have been presented to integrate numerically the IVP defined by the initial state and the incremental relations of the Modified Cam Clay. The computational performance of each of these has been assessed in terms of accuracy and efficiency

so that a more informative decision can be taken when having to choose which of them is more suitable to be implemented in a finite element program.

The integration schemes have been tested against a simple but informative numerical test involving an isotropic straining and both local relative error (incurred in an individual substep) and cumulative relative error (incurred over multiple substeps) have been analysed. The analysis confirms that poorer accuracies are generally achieved by the first order fully implicit backward Euler (BE1) as demonstrated in previous research (e.g. Pedroso & Farias, 2005; Potts & Ganendra, 1994). Such differences in accuracy between BE1 and explicit substepping schemes increase for more stringent values of *STOL*. The computational performance of the four substepping schemes considered has been also assessed in the context of the performance maps proposed in Lloret-Cabot et al. (2016) confirming the suitability of this new form of plotting.

7 REFERENCES

Belytschko, T., Liu, W.K., Moran, B. 2000. *Nonlinear Finite Elements for Continua and Structures*. John Wiley and Sons, Chichester, England.

Coombs, W.M., Crouch, R.S., Augarde, C.E. 2010. Reuleaux plasticity: Analytical backward Euler stress integration and consistent tangent. *Comput. Methods Appl. Mech. Engrg.*, **199**(25–28), 1733-1743.

Coombs, W.M., Crouch, R.S. 2011. Algorithmic issues for three-invariant hyperplastic critical state models. *Comput. Methods Appl. Mech. Engrg.*, **200**(25–28), 2297-2318.

Dormand, J.R., Prince, P.J. 1980. A family of embedded Runge-Kutta formulae. *Journal of Computational and Applied Mathematics*, **6**(1), 19–26.

Farias, M.M., Pedroso, D.M., Nakai, T. 2009. Automatic substepping integration of the subloading tij model with stress path dependent hardening. *Comput Geotech*, **36**, 537-548.

Fehlberg, E. 1969. *Low order classical Runge-Kutta Formulas with step-size control and their application to some heat transfer problems*. NASA Technical Report 315.

Fehlberg, E. 1970. Classical fourth- and lower order Runge-Kutta formulas with stepsize control and their application to heat transfer problems. *Computing*, **6**(1-2), 61-71.

Jeremic, B., Sture, S. 1997. Implicit integrations in elasto-plastic geotechnics. *International Journal for Mechanics of Choesive-Frictional Materials and Structures*, **2**, 165-183.

Lloret-Cabot, M., Sloan, S.W., Sheng, D., Abbo, A.J. 2016. Error behaviour in explicit integration algorithms with automatic substepping. *Int. J. Numer. Methods Eng.*, **108**(9) 1030–1053.

Lloret-Cabot, M., Sloan, S.W., Sheng, D., Abbo, 2017. A.J. Performance Maps: A Simple Way to Verify the Correctness of Explicit Integration Algorithms with Automatic Substepping. *15th Int. Conf. Intern. Assoc. Comp. Meth. Adv. Geomech. (IACMAG)*, Wuhan, China.

Lloret-Cabot, M., Wheeler, S.J., Gens, A., Sloan, S.W. 2021. Numerical integration of an elasto-plastic critical state model for soils under unsaturated conditions. *Comp. Geotech.*, https://doi.org/10.1016/j.compgeo.2021.104299.

Lloret-Cabot, M., Sheng, D. 2022. Assessing the accuracy and efficiency of different order implicit and explicit integration schemes. *Comp. Geotech.*, https://doi.org/10.1016/j.compgeo.2021.104531.

Oliver, J., Huespe, A.E., Cante, J.C. 2008. An implicit/explicit integration scheme to increase computability of nonlinear material and contact/friction problems. *Comput Methods Appl Mech Engrg*, **197**(21),1865-1889.

Pedroso, D.M., Farias, M.M. 2005. Implicit and explicit numerical integration schemes applied to elastoplastic constitutive laws for soils. In: *Proceedings of the 2nd international workshop on new frontiers in computational geotechnics, Gifu University (Japan) and University of Brasilia (Brazil)*; 69–81.

Pedroso, D.M., Sheng, D., Sloan, S.W. 2008. Stress update algorithm for elastoplastic models with nonconvex yield surfaces. *Int. J. Numer. Methods Eng.*, **76**, 2029–2062.

Pérez-Foguet, A., Rodríguez-Ferran, A., Huerta, A. 2001. Consistent tangent matrices for substepping schemes, *Comput. Methods Appl. Mech. Engrg.*, **190**(35-36), 4627-4647.

Potts, D.M., Gens, A. 1985. A critical assessment of methods of correcting for drift from the yield surface in elastoplastic finite element analysis. *Int. J. Numer. Anal. Meth. Geomech.*, **9**, 149–59.

Potts, D.M., Ganendra, D. 1994. An evaluation of substepping and implicit stress points algorithms. *Comput. Methods Appl. Mech. Engrg.* **119**, 341-354.

Sánchez, M., Gens, A., Guimarães, L., Olivella, S. 2008. Implementation algorithm of a generalised plasticity model for swelling clays. *Comp. Geotech.*, **35**(6), 860–871.

Sheng, D., Sloan, S.W., Yu, H.S. 2002. Aspects of finite element implementation of critical state models. *Computational mechanics*, **26**, 185–196.

Sheng, D., Sloan, S.W., Gens, A., Smith, D.W. 2003. Finite element formulation and algorithms for unsaturated soils. Part I: Theory. *Int. J. Numer. Anal. Meth. Geomech.*, **27**, 745–765.

Simo, J.C., Taylor, R.L. 1986. A return mapping algorithm for plane stress elastoplasticity. *Int. J. Numer. Methods Eng.*, **22**(3), 649–670.

Sloan, S.W. 1987. Substepping schemes for the numerical integration of elastoplastic stress-strain relations. *Int. J. Numer. Methods Eng.*, **24**, 893–911.

Sloan, S.W., Abbo, A.J., Sheng, D. 2001. Refined explicit integration of elastoplastic models with automatic error control. *Engineering Computations*, **18**(1-2), pp. 121-154.

Sołowski, W.T., Gallipoli, D. 2010. Explicit stress integration with error control for the Barcelona Basic Model. Part I: Algorithms formulations. *Comp. Geotech.*, **37**(1-2), 59–67.

Sołowski, W.T., Hofmann, M., Hofstetter, G., Sheng, D., Sloan, S. 2012. A comparative study of stress integration methods for the Barcelona Basic Model. *Comp. Geotech.*, **44**, 22–33.